

Document downloaded from:

<http://hdl.handle.net/10251/147734>

This paper must be cited as:

Larroza, A.; López-Lereu, M.; Monmeneu, J.; Gavara-Doñate, J.; Chorro, F.; Bodi, V.; Moratal, D. (2018). Texture analysis of cardiac cine magnetic resonance imaging to detect nonviable segments in patients with chronic myocardial infarction. *Medical Physics*. 45(4):1471-1480. <https://doi.org/10.1002/mp.12783>



The final publication is available at

<https://doi.org/10.1002/mp.12783>

Copyright John Wiley & Sons

Additional Information

Article Type: Research Article

Title: Texture analysis of cardiac cine magnetic resonance imaging to detect non-viable segments in patients with chronic myocardial infarction.

Author names and affiliations:

Andrés Larroza, PhD¹, María P. López-Lereu, MD, PhD², José V. Monmeneu, MD, PhD², Jose Gavara BSc³, Francisco J. Chorro, MD, PhD³, Vicente Bodí, MD, PhD^{3*}, David Moratal, PhD^{4*}

¹ Department of Medicine, Universitat de València, Avda. Blasco Ibáñez 15, 46010.Valencia, Spain.

² Unidad de Imagen Cardíaca, ERESA, Marqués de San Juan 6, 46015. Valencia, Spain.

³ Cardiology Department, Hospital Clínico Universitario, Universitat de València, INCLIVA, Avda. Blasco Ibáñez 17, 46010.Valencia, Spain.

⁴ Center for Biomaterials and Tissue Engineering, Universitat Politècnica de València, Camí de Vera, s/n. 46022. Valencia, Spain.

This article has been accepted for publication and undergone full peer review but has not been through the copyediting, typesetting, pagination and proofreading process, which may lead to differences between this version and the Version of Record. Please cite this article as doi: 10.1002/mp.12783

This article is protected by copyright. All rights reserved.

Corresponding authors:

*David Moratal, PhD

Tel.: (+34) 96.387.70.07 (ext. 88939)

e-mail: dmoratal@eln.upv.es

*Vicente Bodí, MD, PhD

Tel.: (+34) 9639 83357

e-mail: vicente.bodi@uv.es

Abstract

Purpose: To investigate the ability of texture analysis to differentiate between infarcted non-viable, viable, and remote segments on cardiac cine magnetic resonance imaging (MRI).

Methods: This retrospective study included 50 patients suffering chronic myocardial infarction. The data was randomly split into training (30 patients) and testing (20 patients) sets. The left ventricular myocardium was segmented according to the 17-segment model in both cine and late gadolinium enhancement (LGE) MRI. Infarcted myocardium regions were identified on LGE in short-axis views. Non-viable segments were identified as those showing $LGE \geq 50\%$, and viable segments those showing $0 < LGE < 50\%$ transmural extension. Features derived from five texture analysis methods were extracted from the segments on cine images. A support vector machine (SVM) classifier was trained with different

combination of texture features to obtain a model that provided optimal classification performance.

Results: The best classification on testing set was achieved with local binary patterns features using a 2D + t approach, in which the features are computed by including information of the time dimension available in cine sequences. The best overall area under the receiver operating characteristic curve (AUC) were: 0.849, sensitivity of 92% to detect non-viable segments, 72% to detect viable segments, and 85% to detect remote segments.

Conclusion: Non-viable segments can be detected on cine MRI using texture analysis and this may be used as hypothesis for future research aiming to detect the infarcted myocardium by means of a gadolinium-free approach.

Keywords: classification, diagnosis, heart, machine learning, magnetic resonance imaging.

1. Introduction

Texture analysis is defined by various techniques that allow the quantification of patterns and relationships among pixels within an image, therefore obtaining a measure of heterogeneity.

It has been shown that textural patterns, sometimes invisible to the human eye, are present in medical images.¹ Texture analysis has been successfully used for segmentation, detection and classification of healthy tissues and lesions in several medical image modalities.²⁻⁵

Cardiac magnetic resonance imaging (MRI) constitutes the gold standard method for evaluating the structural consequences of myocardial infarction. Typical MRI protocols for chronic ischemic heart disease and viability include cine and late gadolinium enhancement (LGE) acquisitions. Cine modalities provide moving images of the heart and are mainly used

to assess the contractile function, ventricle volumes and ejection fraction. Late gadolinium enhancement (LGE) is the well-established technique to quantify the extent of scar in patients with myocardial infarction.⁶ Existing methods for quantification of scar size rely on the administration of gadolinium to enhance the scarred area and setting an intensity threshold to identify the infarct.⁷

Previous studies reported an improvement in detection of scarred myocardium on LGE images when combining texture and intensity features.^{8,9} Texture analysis was also used to create probability maps using LGE images that aid the visual inspection of the myocardial tissue.¹⁰ Recently, it was reported that texture analysis of non-enhanced cine MRI can differentiate between different etiologies of left ventricular hypertrophy,¹¹ between acute and chronic myocardial infarction,¹² and between controls and patients with subacute and chronic myocardial infarction.¹³

Histological properties of scarred myocardium differ from normal myocardium and in consequence, textural properties should also be different. The fibrosis formation causes distortion of the normal myocardium architecture thus altering the texture properties.¹⁴ We hypothesized that implicit differences between non-viable and remote segments are present in cine MRI and can be detected by the application of texture analysis, so non-viable segments would exhibit different gray-level heterogeneity than remote segments. The potential benefits of this hypothesis imply that myocardial viability could be assessed using solely cine sequences without the need of gadolinium administration for further LGE acquisitions. Contraindications and side effects of gadolinium would be avoided and studies protocols would take shorter time providing significant logistic advantages. The purpose of this study was to investigate the ability of texture analysis of cine MRI to differentiate between non-viable, viable, and remote segments in patients with chronic myocardial infarction.

2. Methods

2.1. Study group

The study group stems from an ongoing registry made up of patients with a first electrocardiogram ST-segment elevation myocardial infarction. In summary, for the present study we retrospectively selected 50 patients (mean age, 61; range, 23 – 80 years old) examined between April 2012 and July 2015 and fulfilling the following inclusion criteria: 1) Successful epicardial reperfusion in the infarct-related artery based on the achievement of a thrombolysis in myocardial infarction (TIMI) flow grade three and residual stenosis < 50% using primary percutaneous intervention within the first six hours after chest pain onset. 2) Absence of significant stenosis (> 50%) in non-culprit arteries at first week and six month-catheterization. 3) Stable clinical course within the first six months.

All patients gave written informed consent and the study protocol was approved by the institutional committee on human research in our institution and conforms to the ethical guidelines of the 1975 Declaration of Helsinki. Baseline characteristics of the study group are displayed in table 1.

The study group was randomly split into training (30 patients) and testing (20 patients) sets. The first group was used to train a classification model capable of distinguishing between non-viable, viable, and remote segments on cine MRI, whereas the second group was used to test the trained classifier.

2.2. Imaging protocol

MRI was performed at 179 ± 12 days after a first electrocardiogram ST-segment myocardial infarction. Images were acquired in breath-hold using a 1.5T MRI scanner (Sonata

Magnetom, Siemens, Erlangen, Germany). Cine images were acquired at rest without contrast, in short-axis views at every 1 cm using steady-state free precession sequences (repetition time/echo time: 3.2/1.6 ms; flip angle: 61°; voxel size: 1.56 × 1.56 × 7 mm). Each short-axis cine sequence consisted of 35 frames. Late gadolinium enhancement (LGE) images were acquired 10 min after the administration of gadolinium at a dose of 0.075 mmol/kg body weight (gadobenate dimeglumine, Multihance, Bracco Diagnostics, Milan, Italy) in projections and locations matched to the cine images. A segmented inversion recovery steady-state free precession was used (repetition time/echo time: 2.5/1.2 ms, flip angle: 45°, voxel size: 1.56 × 1.56 × 7 mm), and inversion time was adapted to null the signal from normal myocardium.

Left ventricle (LV) ejection fraction (%), LV end-diastolic volume index (ml/m²), LV end-systolic volume index (ml/m²) and LV mass (g/m²) were calculated in short-axis views cine images by manual planimetry of endocardial and epicardial borders. Infarct size (% of LV mass) was measured as the percentage of LV mass showing LGE (table 1).

2.3. Myocardial segmentation

Segmentation of the left ventricular myocardium on short-axis views of both cine and LGE images was manually performed by mutual consent of two expert cardiologists (MP.L-L, 16 years of experience; JV.M, 10 years of experience) using the freely available software Segment, version 2.0 (Medviso, Lund, Sweden).¹⁵ Then, the 17-segment AHA model¹⁶ excluding the apex was used to divide the slices into four or six equal segments depending on the slice level. Various slices were used to create the three thick short-axis sections defined by the 17-segment model. Only slices containing myocardium in all 360° were selected. Infarcted myocardium regions were identified in LGE images using the full width and half

maximum (FWHM) technique.⁷ The labeled segments were located on the cine slice with the same spatial location and the closest cardiac phase to that of LGE (end-diastole). Segmentations on cine MRI were propagated to all time frames to allow texture analysis of cine sequences by including the time dimension (2D + t). The latter was performed by copying and pasting each segmentation to the subsequent time frame and by manually editing when necessary to make sure that all segments were properly located. Manual labelling of a target cine MRI volume took around 5 min. per patient, using a standard PC with a 4 GHz Pentium® 4 processor, 16 GB RAM).

Non-viable segments were identified as those showing LGE $\geq 50\%$ transmural extension, segments showing $0 < \text{LGE} < 50\%$ transmural extension were labeled as infarcted but viable and those not showing enhancement were labeled as remote myocardium.¹⁷ In total, 1400 cine MRI segments were defined as ROIs for texture feature extraction: 340 non-viable (24 %), 224 viable (16 %), and 836 remote segments (60 %). Figure 1 shows a general diagram of the proposed methodology.

2.4. Region of interest preprocessing

Preprocessing steps within the segments or regions of interest (ROIs) were implemented to ensure that the outcome of texture analysis truly characterize the intrinsic properties of the images. Images were cropped to focus on the left ventricle and were resampled to a pixel size of $0.5 \times 0.5 \text{ mm}^2$ using bicubic interpolation with an antialiasing filter. We chose the mentioned pixel size to increment the heterogeneous information within the original images without introducing prejudicial noise.¹⁸ Subsequently, non-uniformity correction was applied throughout the myocardium ROI using an additive model.¹⁹ To minimize the influence of

image brightness and contrast variation, normalization was implemented using a technique that remaps the ROI histogram to fit within the intensity mean ± 3 standard deviations.²⁰

2.5. Texture feature extraction

Texture features were calculated for each ROI segment by means of four matrix-based texture analysis methods and local binary patterns (LBP) using public available libraries^{21,22} in Matlab 2015b (The MathWorks Inc, Natick, MA). Table 2 summarizes the calculated features. Formulation of the matrix-based methods, according to the Image Biomarker Standardization Initiative (ISBI),²³ is provided in the supplementary material.²⁴ Please refer to references^{25,26} for a complete description of matrix-based and LBP features.

2D Analysis

Two-dimensional analysis was performed on the end-diastolic cine MRI slice. Texture features were calculated in their rotation invariance form to evade image rotation as a possible source of bias.

In matrix-based methods, only one matrix was computed for each method by simultaneously taking into account the neighboring points at one-pixel distance in four directions: horizontal, vertical, 45° and 135°. It is recommended to optimize the number of gray-levels used for computation of matrix-based features.²⁷ In a preliminary evaluation using the training set, we found that 16 gray-levels yielded the best results among various levels (8, 16, 32, and 64).

For the LBP features, the $LBP_{P,R}$ operator was set to $LBP_{8,1}$, where P is the total number of neighborhood pixels and R is the radius in pixel. Rotation invariance values were used thus the LBP histogram was reduced to 36 bins instead of the original 256.²⁸

2D + t Analysis

To take advantage of the temporal dimension available in cine MRI, texture analysis was also performed in $2D + t$. It was implemented as volumetric 3D texture analysis but using time as the third dimension for each slice. The z dimension was not included because of the very large slice thickness in comparison to pixel size in the available images.

Similar to 2D analysis, only one matrix was computed per method and per slice, by simultaneously considering the neighboring properties of voxels in 13 directions of 3D space.²⁵ A preliminary evaluation showed that 8 gray-levels yielded the best results in our training data, so this value was used for matrix-based features in $2D + t$.

The spatio-temporal LBP known as LBP-TOP is an extension of the LBP operator that was proposed to analyze video sequences.²⁶ The LBP-TOP analyze the video sequence by concatenating the LBP histogram on three orthogonal planes: xy , xt and yt . In our analysis, the $LBP_{P,R}$ operator was used for the three planes and were set to $LBP_{4,1}$, thus obtaining a concatenated histogram of 48 bins.

2.6. Feature selection

Including all the computed features does not always provide the best possible classification accuracy, as the model may suffer from the curse of dimensionality.²⁹ For this reason, we decided to try different subset of features according to the method of calculation, and also to implement a feature selection algorithm to the full set of texture features. The following subset of features were used as input to the classifier.

- **Matrix features:** All texture features derived from the matrix-based methods: gray-level co-occurrence matrix (GLCM), gray-level run-length matrix (GLRLM), gray-level size zone matrix (GLSZM), and neighborhood gray-tone difference matrix (NGTDM).
- **LBP features:** The LBP histogram where each bin represents one feature.
- **Matrix + LBP:** The full set of texture features.
- **Wall thickening (Wth):** The wall thickening (*Wth*), defined as the difference in myocardial thickness between end-diastole and end-systole. The performance using *Wth* solely was taken as reference for comparison with texture-based models.
- **Selected features:** The multiple support vector machine-recursive feature elimination (mSVM-RFE) feature selection technique was implemented to the full set of texture features.³⁰ This is a modified version of the popular SVM-RFE originally proposed for gene selection.³¹ The mSVM-RFE returns a ranking of features according to the score computed from a statistical analysis of weight vectors from various linear SVMs. In our implementation, 5-fold cross-validation with 10 repetitions was used to stabilize the feature selection and the *C* parameter of the linear SVM was set to unity. Different subsets of features were obtained by adding one-by-one the features from most to least important according to the ranking returned by the mSVM-RFE. The subset of features that yielded the best classification (selected features) in the training set was used to train the final model.

2.7. Classification

Classification was performed using a support vector machine (SVM) with Gaussian radial basis function (RBF) kernel (RBF-SVM). Only this classification model was chosen after considering its well-known performance in applications to other datasets.³² Moreover, it is to believe that the features ranked by the mSVM-RFE should perform better with a SVM classifier. Even if a linear SVM is used within the mSVM-RFE to rank features, a radial

RBF-SVM allows more flexibility of the decision boundary by changing the parameters of the RBF kernel. These parameters were tuned through cross-validation, specifically, the kernel parameter σ was chosen from the finite set $\{10^{-2} \dots 10^2\}$ and the RBF-SVM C parameter from the finite set $\{2^{-2} \dots 2^4\}$.³³

2.8. Summary of the learning framework

The framework for training and testing the classification model consisted of the following steps:

- 1) The study group was randomly split into training (30 patients) and testing sets (20 patients).
- 2) The training set was used for model tuning and feature selection and it was split $n = 50$ times by using a 5-fold cross-validation with 10 repetitions. An inner 5-fold cross-validation was used for model tuning. For the implementation of the mSVM-RFE, a middle-loop was included in a nested cross-validation scheme, so the feature selection was always performed in training folds.
- 3) The trained RBF-SVM classifier tuned with the optimal parameters and/or features were then directly applied to the testing set.

Feature values were standardized to unit variance and zero mean across training samples. Some bins of the LBP histograms presented few occurrences for all training samples. These non-zero values were excluded from analysis as they do not contribute for classification.

All classification models were built within a multiclass approach using the one-versus-all technique³⁴. Performance parameters were reported on the testing set by considering each class individually: non-viable, viable and remote myocardium.

The models were trained using the CARET package³⁵ in R language, version 3.3.0 (R Development Core Team, Vienna, Austria) and the mSVM-RFE feature selection was implemented using the code provided by John Colby.³⁶

2.9. Statistical analysis

Receiver operating characteristic (ROC) curves were plotted using the class probabilities of the RBF-SVM, calculated with the method described by Platt.³⁷ Classification accuracy was evaluated with the area under curve (AUC) of the ROC. Sensitivity and specificity were computed for the threshold on the ROC curve that maximizes the product of both parameters. Class probabilities of the best model were also used to analyze the correlation between the infarct percentage measured on LGE MRI and the RBF-SVM probability on cine MRI. The McNemar's test³⁸ was used to compare the performance between models trained with 2D and 2D + *t* features. Student t-test was used to compare AUC with the random classification value (AUC = 0.5) and statistical significance was set at $p < 0.05$. The statistical tests were also implemented in R language.

3. Results

The full ranking of features returned by the mSVM-RFE, averaged over cross-validation folds, is provided in table S1 of the supplementary material. The best 2D feature was derived from the GLSZM texture analysis method and the best 3D feature was from the GLRLM method. The best ranked included features from all texture analysis methods. However, the average ranks are relatively high thus indicating that at each fold of the nested cross-validation different features were selected. The feature profiles shown in figure S1

(supplementary material) indicate that almost all 2D features (67 out of 68) were necessary to achieve optimal classification performance in training data. This indicates that, for the 2D case, the feature selection is not relevant as it does not provide a substantial reduced set of features. For the 2D + t case, 57 out of 87 features were optimal. These optimal number of features were used to train the final model and to test its performance on the testing set. It can be seen that 2D + t features performed better than 2D features in training data.

Feature profiles for each class are presented in figures S2 and S3 (supplementary material) for 2D and 2D + t respectively. In training data, classification performance was better for non-viable than remote segments for both cases. Notably, the classification for viable segments was very poor, which was expected considering that these are the “intermediate” segments that have small percentage of infarcted mass.

Classification performance parameters on testing set are reported in table 3. The AUC values obtained with the selected features are very similar to that of the nested cross-validation profiles. The best overall performance was achieved by combining the selected features with the wall thickening feature (AUC = 0.756) when using the 2D approach. The best overall performance for the 2D + t approach was achieved using only the LBP features (AUC = 0.849).

Chronic scar formation is associated with thinned myocardium; therefore, the wall thickening feature was also used individually to train the RBF-SVM classifier. However, the performance using only this feature was very poor (AUC = 0.561) in comparison to those obtained with texture features. Figure 5 shows a comparison of 2D and 2D + t features that clearly shows how the latter outperforms the 2D approach. This difference was statistically significant for all cases according to the McNemar’s test ($p < 0.01$).

ROC curves for the best models in 2D and 2D + t are shown in figure 3 and figure 4 respectively. The best model was achieved with 2D + t LBP features. AUC values were 0.935, 0.819, and 0.794 for non-viable, viable and remote segments respectively. Notably, classification of viable segments performed better than remote segments on testing set, but sensitivity to detect remote segments (92%) remained higher than the sensitivity to detect viable segments (72%).

Figure 5 was plotted to evaluate if the probability of the RBF-SVM in cine MRI correlates with the infarct percentage measured in LGE MRI. It can be seen that no correlation was found for any of the investigated classes, Pearson correlation coefficient ($r = 0.07$ and $r = -0.36$ for non-viable and viable segments respectively). Figure 6 shows examples of testing cine MRI and the predicted segments compared to the LGE ground truth.

4. Discussion

We have demonstrated that texture analysis has the potential to discriminate between non-viable, viable and remote segments in pre-contrast cine MRI. High discrimination (AUC > 0.8) was achieved using 2D + t texture features extracted from cine MRI, modality in which the scarred myocardium is visually imperceptible in most cases. However, classification was not straightforward as it was necessary the combination of several texture features and an advanced classifier such as the SVM to achieve high discrimination.

In recent years, cardiac MRI has become the gold standard non-invasive imaging technique for a comprehensive evaluation of the structural consequences of myocardial infarction. Beyond the well-established value of cine MRI to accurately quantify relevant parameters in post-infarction patients such as ejection fraction or left ventricular volumes, in this scenario LGE has emerged as a unique tool for calculating the extent of the scar. As derived from

LGE, this variable has been demonstrated to be decisive for predicting left ventricular remodeling, late systolic recovery and patient's outcome.^{39,40} However, the use of LGE involves a prolongation of studies and the administration of contrast. In turn, this implies certain limitations for selected subsets of patients and for cardiac MR labs: i) a significant number of post-infarction patients are still clinically unstable at the time of the study and, as a consequence, they cannot tolerate prolonged studies; ii) the use of gadolinium can induce side effects, especially it can worsen renal function in patients with a certain degree of renal insufficiency; iii) the number of studies per shift in cardiac labs has to be necessarily reduced due to the prolongation of cases in whom LGE sequences have to be used.

Attempts have been made to evaluate myocardial infarction without the need of LGE MRI. Shriki et al.⁴¹ reported that chemical shift artifacts are detectable in cine MRI and are indicative of chronic myocardial infarction. Another study⁴² reported that the edema related to acute myocardial infarction is detectable in cine MRI. These previous studies suggest the possibility to detect infarction in pre-contrast cine MRI. However, their methods rely on the visual assessment of the images that could be challenging in the clinical setting.

Our results are in line with recent studies that implement texture analysis on non-enhanced cardiac cine MRI. Schofield et al.¹¹ studied different etiologies of left ventricular hypertrophy using fine, medium and coarse texture scales on pre-contrast cine MRI. They found that, among the patients with hypertrophic cardiomyopathy, texture features can significantly differentiate those with and without LGE. In a previous study of our group,¹² we found that acute and chronic myocardial infarctions can be differentiated with texture features and a machine learning classifier. In this study, the entire myocardium was used as region of interest, similar approach to that used by Baessler et al.¹³ to differentiate subacute and chronic myocardial scar from healthy controls.

In comparison to previous studies, our current segmented analysis employs rotational invariant texture features and takes advantage of the time dimension of cine sequences by performing the $2D + t$ analysis. Moreover, no specific texture feature able to distinguish between infarcted and remote myocardium was found to be related to those of previous studies. However, based in our findings we believe that a proper combination of different features is necessary to achieve that goal. This is an ongoing area of research in different areas, technique known as Radiomics.⁴³

Weak correlation was found between the percentage of infarct measured in LGE MRI and the probability of the RBF-SVM model in cine MRI, therefore no direct relationship can be obtained and further research is needed aiming to accurately quantify the infarct extent. Nevertheless, the high accuracy obtained with the best classification model motivates the further development of the methodology. Therefore, if it can be validated and extended to detect the scar precisely, relevant benefits for post-infarction patients (less side effects, less time of scanning, better tolerance for unstable patients) and logistic advantages for labs (more studies per unit of time) could be achieved.

The present study shows some limitations: i) images were manually segmented, which could influence the reproducibility of the analysis; ii) images were obtained with the same scanner and acquisition protocol, so further multicenter evaluations with larger study groups is required; iii) No specific subset of features was found to be discriminative according to the applied feature selection technique. Also, 3D and $3D + t$ analysis was not evaluated due to very large slice thickness of the available datasets. Several feature extraction techniques could be incorporated and advanced deep learning approaches could be exploited in future research.

5. Conclusion

This study reinforced the hypothesis that implicit differences between non-viable, viable and remote segments are present in non-enhanced cardiac cine MRI and can be detected by the application of texture analysis.

6. Acknowledgments

This work was supported in part by the Spanish Ministerio de Economía y Competitividad (MINECO) and FEDER funds under grant BFU2015-64380-C2-2-R, by Instituto de Salud Carlos III and FEDER funds under grants FIS PI14/00271 and PIE15/00013 and by the Generalitat Valenciana under grant PROMETEO/2013/007. The first author, Andrés Larroza, was supported by grant FPU12/01140 from the Spanish Ministerio de Educación, Cultura y Deporte (MECD).

7. References

1. Castellano G, Bonilha L, Li LM, Cendes F. Texture analysis of medical images. *Clin Radiol*. 2004;59(12):1061-1069. doi:10.1016/j.crad.2004.07.008.
2. Hodgdon T, Mcinnes MDF, Schieda N, Flood T a, Lamb L, Thornhill RE. Can quantitative CT texture analysis be used to differentiate fat-poor renal angiomyolipoma from renal cell carcinoma on Unenhanced CT images? *Radiology*. 2015;276(3):787-796. doi:10.1148/radiol.2015142215.
3. Larroza A, Moratal D, Paredes-Sánchez A, et al. Support vector machine classification of brain metastasis and radiation necrosis based on texture analysis in MRI. *J Magn Reson Imaging*. 2015;42(5):1362-1368. doi:10.1002/jmri.24913.

- Accepted Article
4. Thevenot J, Hirvasniemi J, Pulkkinen P, et al. Assessment of risk of femoral neck fracture with radiographic texture parameters: a retrospective study. *Radiology*. 2014;272(1):184-191. doi:10.1148/radiol.14131390.
 5. Kassner A, Thornhill RE. Texture analysis: a review of neurologic MR imaging applications. *Am J Neuroradiol*. 2010;31(5):809-816. doi:10.3174/ajnr.A2061.
 6. Pfeiffer MP, Biederman RWW. Cardiac MRI: a general overview with emphasis on current use and indications. *Med Clin North Am*. 2015;99(4):849-861. doi:10.1016/j.mcna.2015.02.011.
 7. Flett AS, Hasleton J, Cook C, et al. Evaluation of techniques for the quantification of myocardial scar of differing etiology using cardiac magnetic resonance. *JACC Cardiovasc Imaging*. 2011;4(2):150-156. doi:10.1016/j.jcmg.2010.11.015.
 8. Engan K, Eftestøl T, Ørn S, Kvaloy JT, Woie L. Exploratory data analysis of image texture and statistical features on myocardium and infarction areas in cardiac magnetic resonance images. In: *32nd Annual International Conference of the IEEE EMBS*. Buenos Aires; 2010:5728-5731. doi:10.1109/IEMBS.2010.5627866.
 9. Kotu LP, Engan K, Eftestøl T, Ørn S, Woie L. Segmentation of scarred and non-scarred myocardium in LG enhanced CMR images using intensity-based textural analysis. In: *33rd Annual International Conference of the IEEE EMBS*. Boston, Massachusetts USA; 2011:5698-5701. doi:10.1109/IEMBS.2011.6091379.
 10. Kotu LP, Engan K, Skretting K, et al. Probability mapping of scarred myocardium using texture and intensity features in CMR images. *Biomed Eng Online*. 2013;12(91):1-19. doi:10.1186/1475-925X-12-91.
 11. Schofield R, Ganeshan B, Kozor R, Nasis A, Endozo R, Ashley M. CMR myocardial texture analysis tracks different etiologies of left ventricular hypertrophy. *J Cardiovasc Magn Reson*. 2016;18(Suppl 1):1-2. doi:10.1186/1532-429X-18-S1-O82.

- Accepted Article
12. Larroza A, Materka A, López-Lereu M, Monmeneu J, Bodí V, Moratal D. Differentiation between acute and chronic myocardial infarction by means of texture analysis of late gadolinium enhancement and cine cardiac magnetic resonance imaging. *Eur J Radiol.* 2017;92:78-83. doi:10.1016/j.ejrad.2017.04.024.
 13. Baessler B, Mannil M, Oebel S, Maintz D, Alkadhi H, Manka R. Subacute and Chronic Left Ventricular Myocardial Scar: Accuracy of Texture Analysis on Nonenhanced Cine MR Images. *Radiology.* 2017;286(1):103-112. doi:10.1148/radiol.2017170213.
 14. Hervas A, Ruiz-Sauri A, de Dios E, et al. Inhomogeneity of collagen organization within the fibrotic scar after myocardial infarction: Results in a swine model and in human samples. *J Anat.* 2016;228(1):47-58. doi:10.1111/joa.12395.
 15. Heiberg E, Sjögren J, Ugander M, Carlsson M, Engblom H, Arheden H. Design and validation of Segment--freely available software for cardiovascular image analysis. *BMC Med Imaging.* 2010;10:1-13. doi:10.1186/1471-2342-10-1.
 16. Cerqueira MD, Weissman NJ, Dilsizian V, et al. Standardized myocardial segmentation and nomenclature for tomographic imaging of the heart. *Circulation.* 2002;105(4):539-542. doi:10.1067/mnc.2002.123122.
 17. Bodí V, Sanchis J, López-lereu MP, et al. Usefulness of a comprehensive cardiovascular magnetic resonance imaging assessment for predicting recovery of left ventricular wall motion in the setting of myocardial stunning. *J Am Coll Cardiol.* 2005;46(9):1747-1752. doi:10.1016/j.jacc.2005.07.039.
 18. Rangayyan RM, Nguyen TM, Ayres FJ, Nandi AK. Effect of pixel resolution on texture features of breast masses in mammograms. *J Digit Imaging.* 2010;23(5):547-553. doi:10.1007/s10278-009-9238-0.
 19. Materka A, Strzelecki M. On the importance of MRI nonuniformity correction for texture analysis. In: *Signal Processing: Algorithms, Architectures, Arrangements, and Applications*

- (SPA). Poznan; 2013:118-123.
20. Collewet G, Strzelecki M, Mariette F. Influence of MRI acquisition protocols and image intensity normalization methods on texture classification. *Magn Reson Imaging*. 2004;22(1):81-91. doi:10.1016/j.mri.2003.09.001.
 21. Vallières M. MATLAB programming tools for radiomics analysis. <https://github.com/mvallieres/radiomics>. Accessed December 15, 2017.
 22. Zhao G, Pietikainen M. Center for machine vision and signal analysis. University of Oulu. <http://www.cse.oulu.fi/CMV/Downloads/LBP Matlab>. Accessed December 15, 2017.
 23. Zwanenburg A, Leger S, Vallières M, Löck S, Image biomarker standardisation initiative. 2017;(November). <http://arxiv.org/abs/1612.07003>.
 24. See supplementary material at <http://dx.doi.org> for the formulas of matrix-based texture features and for the supplementary table and figures.
 25. Vallières M, Freeman CR, Skamene SR, El Naqa I. A radiomics model from joint FDG-PET and MRI texture features for the prediction of lung metastases in soft-tissue sarcomas of the extremities. *Phys Med Biol*. 2015;60(14):5471-5496. doi:10.1088/0031-9155/60/14/5471.
 26. Zhao G, Pietikainen M. Dynamic texture recognition using local binary patterns with an application to facial expressions. *IEEE Trans Pattern Anal Mach Intell*. 2007;29(6):915-928. doi:10.1109/TPAMI.2007.1110.
 27. Larroza A, Bodí V, Moratal D. Texture analysis in magnetic resonance imaging: review and considerations for future applications. In: Constantinides C, ed. *Assessment of Cellular and Organ Function and Dysfunction Using Direct and Derived MRI Methodologies*. Rijeka, Croatia: Intech; 2016:75-106. doi: 10.5772/64641.
 28. Ojala T, Pietikäinen M, Mäenpää T. A generalized local binary pattern operator for multiresolution gray scale and rotation invariant texture classification. In: *Second International*

Conference on Advances in Pattern Recognition. London; 2001:397-406. doi:10.1007/3-540-44732-6_41.

29. Guyon I, Elisseeff A. An introduction to variable and feature selection. *J Mach Learn Res*. 2003;3:1157-1182. doi:10.1162/153244303322753616.
30. Duan KB, Rajapakse JC, Wang H, Azuaje F. Multiple SVM-RFE for gene selection in cancer classification with expression data. *IEEE Trans Nanobioscience*. 2005;4(3):228-233. doi:10.1109/TNB.2005.853657.
31. Guyon I, Weston J, Barnhill S, Vapnik V. Gene selection for cancer classification using support vector machines. *Mach Learn*. 2002;46:389-422. doi:10.1023/A:1012487302797.
32. Fernández-Delgado M, Cernadas E, Barro S, Amorim D. Do we need hundreds of classifiers to solve real world classification problems? *J Mach Learn Res*. 2014;15:3133-3181. <http://jmlr.org/papers/v15/delgado14a.html>.
33. Wang S, Summers RM. Machine learning and radiology. *Med Image Anal*. 2012;16(5):933-951. doi:10.1016/j.media.2012.02.005.
34. James G, Witten D, Hastie T, Tibshirani R. *An Introduction to Statistical Learning with Applications in R*. New York, NY, USA: Springer; 2006. doi:10.1016/j.peva.2007.06.006.
35. Kuhn M. Building predictive models in R using the caret package. *J Stat Softw*. 2008;28:1-26.
36. Colby J. (multiple) Support Vector Machine Recursive Feature Elimination - mSVM-RFE. <http://www.colbyimaging.com/wiki/statistics/msvm-rfe>. Accessed December 15, 2017.
37. Platt J. Probabilistic outputs for support vector machines and comparisons to regularized likelihood methods. In: Smola J, Barlett P, Schölkopf B, Schuurmans D, eds. *Advances in Large Margin Classifiers*. Vol 10. Cambridge, MA: MIT Press; 1999:61-74. doi:10.1.1.41.1639.
38. Salzberg SL. On comparing classifiers: pitfalls to avoid and a recommended approach. *Data*

Min Knowl Discov. 1997;1:317-328.

39. Bodí V, Husser O, Sanchis J, et al. Contractile reserve and extent of transmural necrosis in the setting of myocardial stunning: comparison at cardiac MR imaging. *Radiology.* 2010;255(3):755-763. doi:10.1148/radiol.10091191.
40. Bodi V, Monmeneu J V, Ortiz-Perez JT, et al. Prediction of reverse remodeling at cardiac MR imaging soon after first ST-segment-elevation myocardial infarction: results of a large prospective registry. *Radiology.* 2016;278(1):54-63. doi:10.1148/radiol.2015142674.
41. Shriki JE, Surti KS, Farvid AF, et al. Chemical shift artifact on steady-state free precession cardiac magnetic resonance sequences as a result of lipomatous metaplasia: a novel finding in chronic myocardial infarctions. *Can J Cardiol.* 2011;27(5):664.e17-664.e23. doi:10.1016/j.cjca.2010.12.074.
42. Goldfarb JW, Mclaughlin J, Gray CA, Han J. Cyclic cine-balanced steady-state free precession image intensity variations: implications for the detection of myocardial edema. 2011;33(3):573-581. doi:10.1002/jmri.22368.
43. Gillies RJ, Kinahan PE, Hricak H. Radiomics: images are more than pictures, they are data. *Radiology.* 2016;278(2):563-577. doi:10.1148/radiol.2015151169.

Figure. 1. General diagram of our texture-based approach to differentiate between non-viable, viable, and remote segments. In the training phase, late gadolinium enhancement (LGE) MRI was used as reference to define regions of interest (ROIs) in the corresponding cine MRI slice. Texture features were extracted from segments on cine MRI and were used to train a support vector machine (SVM) classifier.

Figure 2. Barplot comparing the AUC values on testing set for 2D and 2D + t features on testing set for each subset of features. 2D + t features provided larger values in all cases with statistical significance according to the McNemar's test ($p < 0.01$).

Figure 3. ROC curves for the best model using 2D features (With + selected features). One ROC curve for each class is shown according to the one-versus-all technique. The circles on the curves indicate the optimal operating point that maximizes the product between sensitivity and specificity.

Figure 4. ROC curves for the best models using 2D + t features (LBP). One ROC curve for each class is shown according to the one-versus-all technique. The circles on the curves indicate the optimal operating point that maximizes the product between sensitivity and specificity.

Figure 5. Scatter plot on testing set for the infarct percentage measured in LGE MRI versus the probability of the RBF-SVM classifier as predicted in cine MRI. The RBF-SVM predictions for the best model (LBP features in 2D + t) were used.

Figure 6. Examples of images on testing set and the predictions using the LBP features in 2D + t . Scar (yellow) is represented on the ground truth LGE images. Segments predicted as non-viable are colored in red, those predicted as viable in blue and those predicted as remote in green. Arrows indicate the incorrectly predicted segments. Top row shows a correctly

classified image, the inferoseptal segment is covered by less than 50% of scar and it was predicted as viable. The middle row shows a small scar that covers slightly more than 50% of the segment and it was incorrectly classified as viable. The two non-viable segments of the bottom row were correctly classified but the viable segment was incorrectly predicted as remote.

Table 1. Baseline characteristics of the study group and cardiac magnetic resonance parameters.

Number of patients	50
<u>Baseline characteristics</u>	
Age (years)	61 ± 12
Male sex (%)	45 (90)
Diabetes mellitus (%)	13 (26)
Hypertension (%)	17 (34)
Dyslipidemia (%)	16 (32)
Current Smoker (%)	10 (20)
Heart rate (beats per min)	82 ± 11
Systolic blood pressure (mm Hg)	139 ± 26
<u>Magnetic resonance parameters</u>	
LV Ejection fraction (%)	51 ± 16
LV End-diastolic volume index (ml/m ²)	86 ± 31
LV End-systolic volume index (ml/m ²)	45 ± 29
LV mass (g/m ²)	73 ± 19
Infarct size (% of LV mass)	21 ± 12
<u>Infarct location</u>	
Anterior (%)	38 (76)
Inferior (%)	8 (16)
Other (%)	4 (8)

Continuous variables are expressed as mean ± standard deviation. LV: Left ventricle.

Table 2. List of texture features used in the present study.

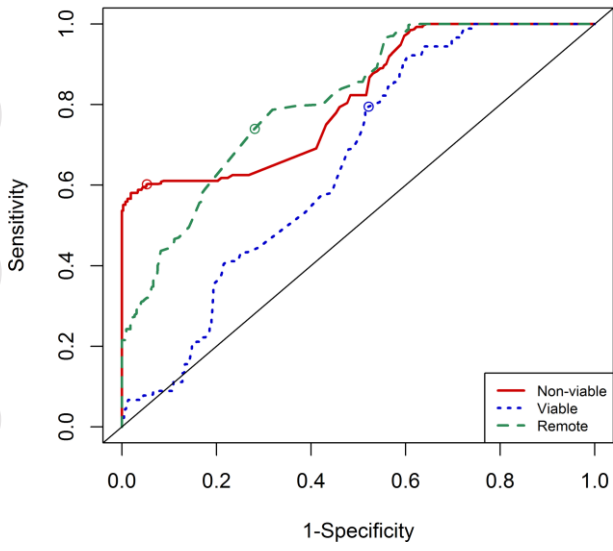
Method	Features	# 2D	# 2D+t
Gray-level co-occurrence matrix (GLCM)	Entropy, Energy, Correlation, Homogeneity, Dissimilarity, Variance, Sum average, Contrast.	8	8
Gray-level run-length matrix (GLRLM)	Run percentage (RP), Short run emphasis (SRE), Gray-level nonuniformity (GLN), Run-length variance (RLV), Run-length nonuniformity (RLN), Gray-level variance (GLV), Low gray-level run emphasis (LGRE), High gray-level run emphasis (HGRE), Short run low gray-level emphasis (SRLGE), Long run emphasis (LRE), Long run low gray-level emphasis (LRLGE), Long run high gray-level emphasis (LRHGE), Short run high gray-level emphasis (SRHGE).	13	13
Gray-level size zone matrix (GLSZM)	Large zone emphasis (LZE), Gray-level nonuniformity (GLN), Zone-size nonuniformity (ZSN), Zone percentage (ZP), Small zone emphasis (SZE), Zone-size variance (ZSV), High gray-level zone emphasis (HGZE), Small zone low gray-level emphasis (SZLGE), Low gray-level zone emphasis (LGZE), Small zone high gray-level emphasis (SZHGE), Large zone low gray-level emphasis (LZLGE), Large zone high gray-level emphasis (LZHGE), Gray-level variance (GLV).	13	13
Neighborhood gray-tone difference matrix (NGTDM)	Busyness, Coarseness, Complexity, Contrast, Strength.	5	5
Local Binary Patterns (LBP)	2D: $P=8$ and $R=1$, 2D+t: $P=4$ and $R=1$ in three orthogonal planes.	36	48

Table 3. Classification performance parameters on testing set using the trained RBF-SVM classifier.

Feature subset	# Features	Overall AUC	Non-viable			Viable			Remote		
			AUC	Sens	Spec	AUC	Sens	Spec	AUC	Sens	Spec
Wall thickening	1	0.561	0.601	0.676	0.476	0.565	0.611	0.572	0.518	0.476	0.601
Matrix	39	0.753	0.733	0.507	0.976	0.715	0.900	0.612	0.813	0.706	0.730
LBP	29	0.727	0.889	0.977	0.636	0.563	0.377	0.814	0.730	0.787	0.650
2D Matrix + LBP	68	0.737	0.810	0.580	0.981	0.635	0.788	0.459	0.765	0.694	0.650
Selected features	67	0.755	0.815	0.580	0.976	0.656	0.755	0.536	0.795	0.736	0.681
Wth + SF	68	0.756	0.811	0.602	0.948	0.651	0.800	0.485	0.805	0.754	0.716
Matrix	39	0.811	0.810	0.647	0.797	0.822	0.855	0.748	0.802	0.631	0.911
LBP	48	0.849	0.935	0.926	0.799	0.819	0.722	0.789	0.794	0.850	0.584
2D + t Matrix + LBP	87	0.822	0.906	0.757	0.877	0.784	0.922	0.621	0.776	0.655	0.752
Selected features	57	0.807	0.911	0.794	0.875	0.752	0.877	0.587	0.759	0.631	0.761
Wth + SF	58	0.820	0.939	0.970	0.757	0.738	0.866	0.561	0.783	0.613	0.827

AUC: area under the ROC curve, LBP: local binary patterns, SF: selected features, Wth: wall thickening. Sensitivity and specificity were computed according to the optimal threshold on the ROC curve that maximizes the product between both parameters.

2D - Cine CMR



2D + t - Cine CMR

